

Surface-Related States in Oxidized Silicon Nanocrystals Enhance Carrier Relaxation and Inhibit Auger Recombination

Andreas Othonos · Emmanouil Lioudakis ·
A. G. Nassiopoulou

Received: 15 July 2008 / Accepted: 14 August 2008 / Published online: 3 September 2008
© to the authors 2008

Abstract We have studied ultrafast carrier dynamics in oxidized silicon nanocrystals (NCs) and the role that surface-related states play in the various relaxation mechanisms over a broad range of photon excitation energy corresponding to energy levels below and above the direct bandgap of the formed NCs. Transient photoinduced absorption techniques have been employed to investigate the effects of surface-related states on the relaxation dynamics of photogenerated carriers in 2.8 nm oxidized silicon NCs. Independent of the excitation photon energy, non-degenerate measurements reveal several distinct relaxation regions corresponding to relaxation of photoexcited carriers from the initial excited states, the lowest indirect states and the surface-related states. Furthermore, degenerate and non-degenerate measurements at difference excitation fluences reveal a linear dependence of the maximum of the photo-induced absorption (PA) signal and an identical decay, suggesting that Auger recombination does not play a significant role in these nanostructures even for fluence generating up to 20 carriers/NC.

Keywords Silicon nanocrystals · Carrier dynamics · Ultrafast spectroscopy · Surface-related states · Auger recombination

Introduction

Silicon is the basic material of today's integrated circuit technology. However, one of the major drawbacks of this indirect gap semiconductor is its inability to efficiently emit light. The observation of efficient photoluminescence (PL) from porous silicon [1–4] and silicon nanocrystals a few years ago [5] has provided hope for Si-based optoelectronics and has stirred research interest in the area of Si nanostructures as a potential candidate for silicon-based emission devices [6–9]. It is well known that semiconductor nanocrystals (NCs) exhibit interesting size-dependent properties, mainly due to the large fraction of surface atoms to the total number of atoms in the NC and quantum size effects that may allow tuning of the light emission peak from such nanostructures. Although there have been different forms of Si-NCs (in nanostructured porous silicon or embedded in different insulating matrices), Si-NCs embedded in a amorphous SiO₂ matrix [10, 11] have gained considerable interest due to their PL stability with time for light emission applications and their nanoelectronics applications. Since the demonstration of this type of Si-NCs, there has been a significant research interest in their photoluminescence properties, with little emphasis on the ultrafast carrier dynamics [12]. In particular, there has been no comprehensive study of the effects of surface-related states on the relaxation mechanisms in oxidized Si-NCs over a broad excitation energy range which covers energy states located below and above the direct critical points of the first Brillouin zone of these structures. In view of this lack of information, transient photoinduced absorption measurements have been utilized to investigate and time-resolve the various relaxation mechanisms following photoexcitation in the range of 4.2–3.1 eV, corresponding to direct and indirect (phonon assisted) excitations for 2.8 nm

A. Othonos (✉) · E. Lioudakis
Department of Physics, Research Center of Ultrafast Science,
University of Cyprus, P.O. Box 20537, 1678 Nicosia, Cyprus
e-mail: othonos@ucy.ac.cy

A. G. Nassiopoulou
IMEL/NCSR Demokritos, Terma Patriarchou Grigoriou, Aghia
Paraskevi, 153 10 Athens, Greece

oxidized Si-NCs. The presence of surface-related states appears to play a crucial role in the fast relaxation dynamics of carriers inhibiting the non-radiative Auger recombination even at excitation fluence that generates 20 carriers/NCs.

Experimental Procedure

In this work, the dynamical behavior of oxidized Si-NCs following ultrashort pulse excitation is investigated through the temporal behavior of reflectivity and transmission [13]. The source of excitation consists of a self mode-locked Ti: Sapphire oscillator generating 45 fs pulses at 800 nm. A chirped pulsed laser amplifier based on a regenerative cavity configuration is used to amplify the pulses to approximately 2.2 mJ at a repetition rate of 5 kHz. Part of the energy was used to pump an Optical Parametric Amplifier (OPA) for generating UV ultrashort pulses, and a second part of the energy was used to frequency double the fundamental to 400 nm using a non-linear BBO crystal. A half wave plate and a polarizer in front of the non-linear crystal were utilized to control the intensity of the pump incident on the sample. A small part of the fundamental energy was also used to generate a super continuum white light by focusing the beam on a sapphire plate. An ultrathin high reflector at 800 nm was used to reject the residual fundamental light from the generated white light to eliminate the possibility of effects by the probe light. The white light probe beam is used in a non-collinear geometry, in a pump-probe configuration where the pump beam was generated from either the OPA or the frequency doubling of the fundamental. Optical elements such as focusing mirrors were utilized to minimize dispersion effects and thus not broadening the laser pulse. The reflected and transmission beams are separately directed onto their respective silicon detectors after passing through a bandpass filter selecting the probe wavelength from the white light. The differential reflected and transmission signals were measured using lock-in amplifiers with reference to the optical chopper frequency of the pump beam. The temporal variation in the PA is extracted using the transient reflection and transmission measurements, which is a direct measure of the photoexcited carrier dynamics within the probing region [12, 13]. Precision measurements of the spot size on the sample of the pump beam along with measurements of reflection and transmission at the pump wavelength provided accurate estimation of the absorbed fluence ($<250 \mu\text{J}/\text{cm}^2$) for each experiment in this work.

The 2.8 nm size of NCs under investigation are formed with the oxidation at 900 °C of an ultrathin nanocrystalline silicon film with thickness 5 nm on a transparent quartz substrate. The growth of the nanocrystalline silicon film on

quartz was performed by low pressure chemical vapor deposition (LPCVD) of silicon at 610 °C, 300 mTorr. The nanograins within the amorphous film had a vertical size of 5 nm and mean lateral size of 11.3 nm [14]. After oxidation, the vertical NC size was reduced to 2.8 nm, while the mean lateral size was reduced to 6.5 nm. Well-separated nanocrystals embedded in the SiO_2 matrix were thus obtained.

Results and Discussion

Transient degenerate absorption measurements obtained in the UV region of the spectra covering the range of 4.2–3.1 eV for the Si-NCs are shown in Fig. 1a. Given the variation in the linear absorption as a function of excitation

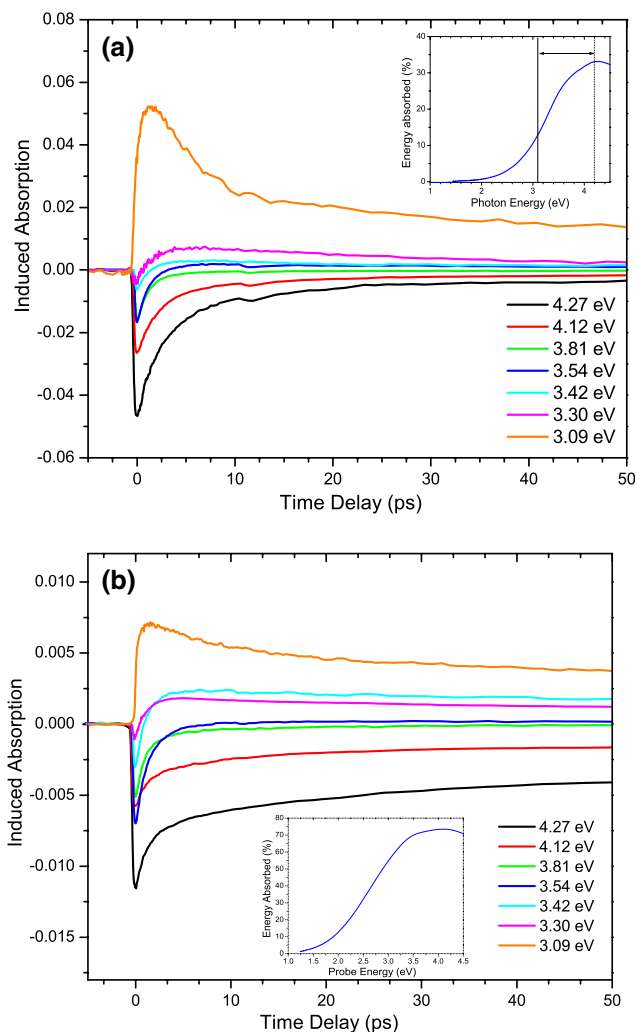


Fig. 1 Degenerate time-resolved absorption measurements of (a) 2.8 nm Si-NCs (b) 5 nm ultrathin nanocrystalline silicon film. The insets show the percentage of the absorbed incident energy by the sample over the range of excitation 3.1–4.2 eV

photon energy (see inset of Fig. 1a) the incident fluences were varied in order that ~ 20 carriers/NC were generated for all photon energies.

Time-resolved absorption measurements for the as-grown ultrathin nanocrystalline silicon film (5 nm thickness) are also shown in Fig. 1b for comparison purposes. We should point out that the 2.8 nm oxidized Si-NCs sample was fabricated from an identical film when oxidized at high temperature. The insets in both figures depict the linear absorption behavior corresponding to the percentage of the absorbed incident energy as a function of photon energy for each sample.

It is clearly evident from the Si-NCs time-resolved data that there is a sharp drop in the induced absorption signal followed by a multi-exponential recovery toward equilibrium. However, with decreasing photon energy the minimum signal decreases and eventually a positive contribution to the absorption change becomes apparent. This observed complex behavior in the time-resolved data is attributed to state filling (SF) and photoinduced absorption (PA) effects. Following excitation of carriers from the ground to excited states, the occupation of the excited states results in bleaching of the absorption (SF) which appears as a negative absorption change. Furthermore, excitation of the carriers with an ultrafast pulse will provide the means of monitoring the temporal evolution of the occupied states and more specifically the relaxation of the photoexcited carriers out of these states. In addition to the negative SF described above, there are also effects due to secondary excitations of the photogenerated carriers to higher energy states introduced by the probing laser pulse. This mechanism will be observed as a positive change in absorption (PA) with its strength depending on the coupling efficiency and the number of carriers present in the initial coupled energy state. In time-resolved absorption measurements, both effects maybe present with their relative contribution depending on the energy states of the material under investigation. For the Si-NCs used in this work, SF is the main contribution for photon energies between 4.27 and 3.42 eV, where direct excitation occurs. On the other hand, for photon energies of 3.3 eV and lower a highly unlikely phonon assisted process must occur to observe SF, thus making the positive PA more likely to observe.

The exponential recovery of the SF is attributed to carriers moving out of the excitation region to the various surface-related states located near the excitation region. The multiple exponential behavior is mainly due to some type of bottleneck effect of the carriers moving through the surface-related states toward the indirect valleys and a contribution in the signal from the presence of PA. Here we should point out that similar effects are also observed in the 5 nm ultrathin film, where SF and PA are evident. The two main noticeable differences between the transient

absorption measurements of the Si-NCs and the film sample are the larger SF effect and the faster recovery toward equilibrium of the Si-NCs. Both differences are attributed to the size of the Si-NCs and the significant role of oxygen-related states surrounding the NCs. Specifically, the larger state SF is mainly due to smaller number of states available in the NC and the faster recovery is due to the larger fraction of surface to volume atoms making the contribution of the surface-related states more important in the NC.

In an attempt to help the reader understand the observed transient absorption behavior of the Si-NCs, in Fig. 2 we show a simplified schematic diagram of a model that is used to explain the excitation and subsequent relaxation of the photogenerated carriers. The blue vertical arrow indicated with (a) corresponds to the direct excitation (>3.4 eV) of carriers into the conduction band whereas the orange arrow indicated with (b) corresponds to the phonon-assisted excitation of carriers (3.1–3.3 eV). In both cases, the energetic carriers relax to the lowest indirect state through the available NCs and surface-related states via emission of phonons. The characteristic times shown in the schematic diagram were obtained from fittings of the experimental PA data to multi-exponential decays.

Time-resolved non-degenerate measurements were also performed for the 2.8 nm Si-NC sample over the same excitation photon energy range as in the degenerate measurements. However, unlike the degenerate measurement, probing was carried out using a super continuum white light with photon energies ranging between 1.26 and 2.75 eV. Figure 3a–c shows the normalized transient absorption measurements for three different photon excitation energies, namely at 4.13, 3.5, and 3.09 eV, respectively. The pump

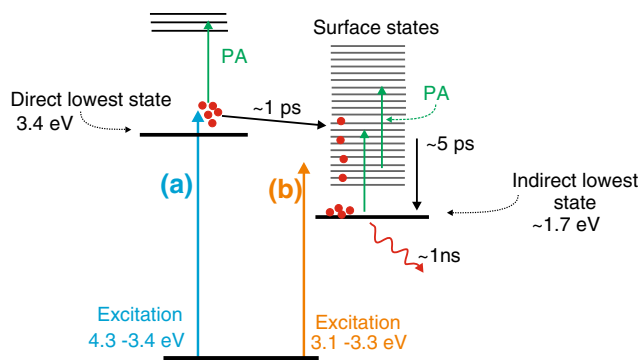


Fig. 2 This figure shows a schematic diagram of the model utilized to explain the excitation and subsequent relaxation in the Si-NCs following femtosecond pulse excitations. The vertical arrows indicate the direct excitation (a) and indirect phonon assisted excitation (b) of the carriers to the conduction band. The short vertical arrows (PA) pointing upward represent secondary excitations of the carriers by the probe pulse

fluence utilized in these measurements was the same as that in degenerate measurements, corresponding to an estimation excitation of 20 carriers/NC. Here, it is also important to point out that measurements with much lower fluence show similar behavior for all probing photon energies.

Independent of photon excitation energy all the transient absorption measurements seen in Fig. 3 show a sharp rise to a maximum change in absorption and then a multi-exponential decay toward equilibrium. This decay persists for a few tens of picoseconds depending on the probing photon energy. The observed absorption changes are clearly due to secondary excitations by the probing photons of photoexcited carriers which are distributed throughout the available energy states in the Si-NCs (see case (b) in Fig. 2). What is interesting is the fact that observed dynamics are independent of the excitation photon energy. Fitting parameters to the time-resolved measurements for 4.13 eV excitation and different probing photon energies (Fig. 3a) with a multi-exponential decay ($A(t) = \alpha_1 e^{-t/\tau_1} + \alpha_2 e^{-t/\tau_2} + \alpha_3 e^{-t/\tau_3}$) are shown in Table 1. We should point out that at other photon excitations in this work we observed similar values for the fitting parameters.

Next, we will explain the various decays and mechanisms of the observed time-resolved measurements based on the model shown in Fig. 2. The fast exponential decay ($\tau_1 \sim 1\text{--}0.6$ ps) seen for the 2.25 eV and smaller probing photon energies corresponds to the carrier transferring time from the excitation region (pump 4.13 eV, see case (a) in Fig. 2) to the surrounding surface-related states. This is further supported by the sharp rise (pulse width limited) to a maximum PA signal seen for probing photon energies smaller than 2.25 eV, suggesting that once the carriers are generated they provide PA signal. On the other hand, the delay (~ 1 ps) in reaching the maximum PA signal observed for the probing photon energy of 2.75 eV suggests that the PA in this case occurs at the surface-related states after the carriers have moved from their initial excitation region. It is interesting to point out that the decay component for the 2.75 eV probing is relatively long. The fitting initial time constant is of the order of 5 ps. This clearly suggests that the observable PA probing is carried out not from the initial excited states but most likely from the nearby surface-related states as shown in the schematic of Fig. 2. We believe that measured ~ 5 ps decay is associated with the time that the photoexcited carriers require to reach the lowest indirect state. This is further supported by the degenerate time-resolved absorption measurements at 3.09 eV (see Fig. 1a, which corresponds to Fig. 2b), where the excitation is below the direct energy states, and similar time constant (~ 5.5 ps) is evident which most likely comes from PA from the surface-related states. Finally, the long decay component ~ 1 ns which is observed for the 2.75 eV probing energy is attributed to

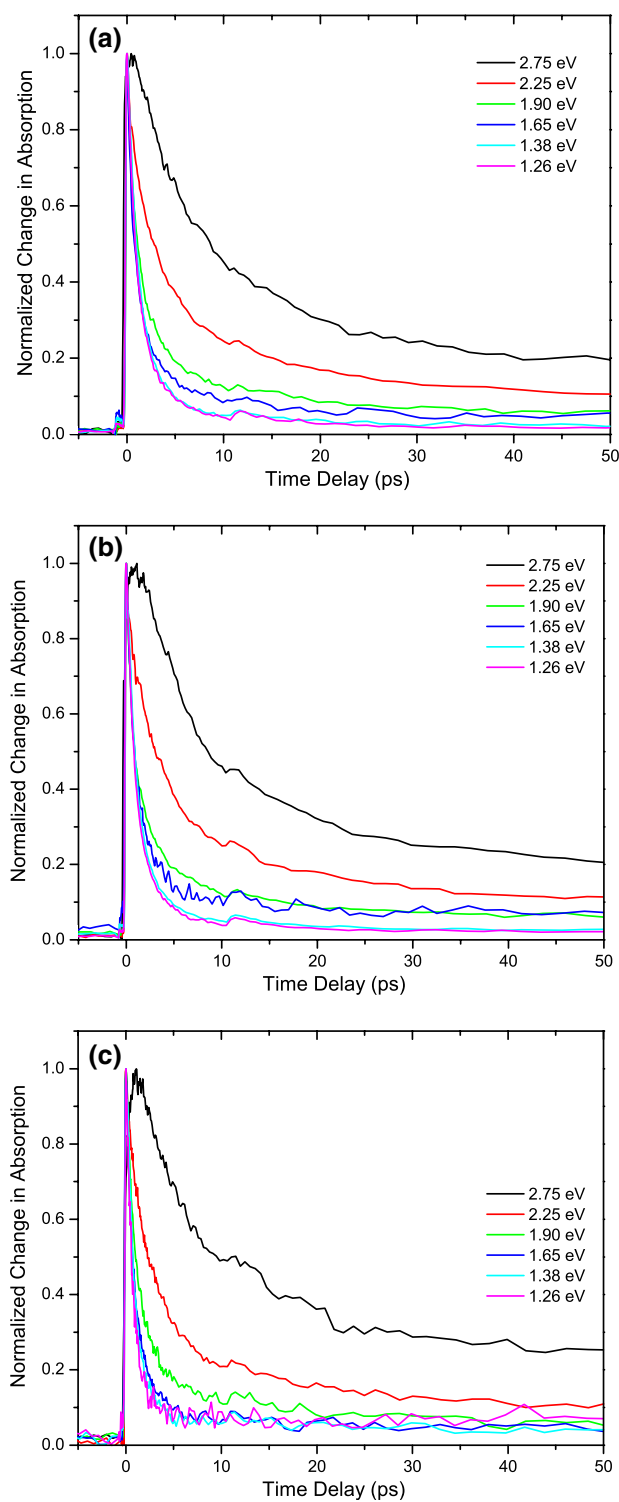
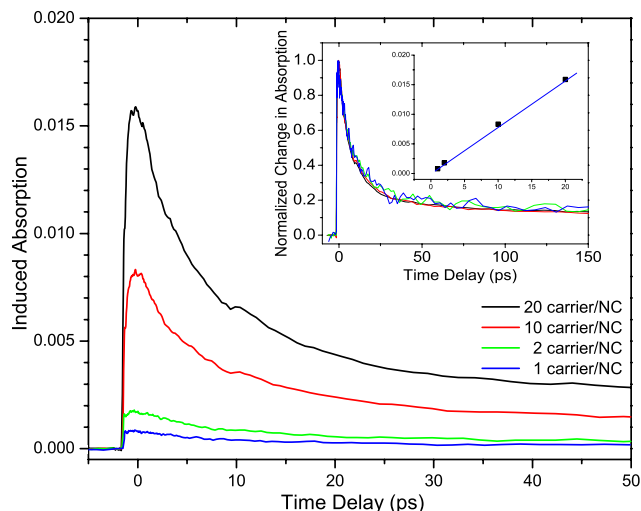


Fig. 3 Transient PA measurements for the Si-NCs at different excitation photon energies (**a**) 4.13 eV, (**b**) 3.5 eV, and (**c**) 3.1 eV. The Si-NC sample was probed with a super continuum white light with photon energies ranging between 2.75 and 1.26 eV

radiative recombination of the carriers after reaching the lowest indirect energy state of the Si-NCs, as indicated in Fig. 2.

Table 1 Fitting parameters obtained from the experimental data of Fig. 3a using a three exponential decay model

Pump (eV) 4.13	Probe (eV)				
	2.75	2.25	1.95	1.65	1.26
α_1	0.46	0.31	0.65	0.65	0.75
τ_1 (ps)	5.1	1.0	0.79	0.59	0.86
α_2	0.36	0.49	0.35	0.35	0.25
τ_2 (ps)	15.7	5.8	4.4	3.2	3.4
α_3	0.18	0.17	–	–	–
τ_3 (ps)	982	127	–	–	–

**Fig. 4** Transient PA intensity measurements for the Si-NCs at 4.13 eV excitation and probe at 2.75 eV. The measurements were taken at 250, 125, 25, and 12.5 $\mu\text{J}/\text{cm}^2$ corresponding to an estimation of 20, 10, 2, and 1 carriers/NC. The inset shows the normalized data depicting the same temporal behavior for all intensities as well as the linear behavior of the maximum absorption changes

Given the size of the NCs it is important to investigate the effect of generation of multiple carriers within the crystals. In what follows, we will describe some of the time-resolved PA intensity measurements carried out in this work. Figure 4 shows data corresponding to photoexcitation of the Si-NCs with 4.13 eV femtosecond pulses and probing with 2.75 eV photons. The fluence shown corresponds to an estimated carrier generation of 20, 10, 2, and 1 carriers/NC. What is interesting is that the maximum absorption changes appear to be linearly dependent on the fluence. Furthermore, the temporal behavior is identical for all fluences as evident from the normalized change in the absorption shown in the inset. This behavior is independent of excitation and probing photon energy utilized in this work.

The observed behavior suggests that Auger recombination does not appear to play any role at carrier densities up to 20 carriers/NC. This is rather surprising given that due to the NC confinement the multiple carrier interaction would

be more pronounced. This unexpected behavior is attributed to the existence of a large fraction of surface-related states surrounding the core of NCs, which inhibit the Auger recombination. The fast transfer of carriers to these states (~ 1 ps) minimizes the probability for these non-linear interactions.

Conclusions

We have investigated femtosecond carrier dynamics in oxidized 2.8 nm Si-NCs using transient degenerate and non-degenerate absorption measurements. A fast carrier transferring time (~ 1 ps) was observed from the initial direct excited states (Γ points in the first Brillouin zone) to the surface-related states surrounding the core of Si-NCs. The relaxation of carriers within the surface-related states (~ 5 ps) appears to be governed by some type of bottleneck effect moving the carriers through the surface-related states toward the indirect energy states of Si-NCs. Furthermore, a long relaxation time (~ 1 ns) was observed from the indirect energy states which is due to the radiative recombination of carriers. Finally, intensity measurements revealed a linear dependence of the PA signal on the photon flux for degenerate and non-degenerate measurements, suggesting that Auger recombination does not play a significant role in these nanostructures for fluences generating up to 20 carriers/NC. This is attributed to the fact that the initial excited carriers move very fast to the surface-related states inhibiting non-linear effects such as Auger recombination.

Acknowledgments The work in this article was partially supported by the research programs ERYAN/0506/04 and ERYNE/0506/02 funded by the Cyprus Research Promotion Foundation in Cyprus.

References

1. L. Canham, *Appl. Phys. Lett.* **57**, 1046 (1990). doi:[10.1063/1.103561](https://doi.org/10.1063/1.103561)
2. H. Koyama, N. Koshida, *J. Appl. Phys.* **74**, 6365 (1993). doi:[10.1063/1.355160](https://doi.org/10.1063/1.355160)
3. H. Mizuto, H. Koyama, N. Koshida, *Appl. Phys. Lett.* **69**, 3779 (1996). doi:[10.1063/1.116996](https://doi.org/10.1063/1.116996)
4. A.G. Cullis, L.T. Canham, P.D.J. Calcott, *J. Appl. Phys.* **82**, 909 (1997). doi:[10.1063/1.366536](https://doi.org/10.1063/1.366536)
5. T. Shimizu-Iwayama, M. Ohshima, T. Niimi, S. Nakao, K. Saitoh, T. Fujita et al., *J. Phys. Condens. Matter* **5**, L375 (1993). doi:[10.1088/0953-8984/5/31/002](https://doi.org/10.1088/0953-8984/5/31/002)
6. F. Iacona, D. Pacifici, A. Irrera, M. Miritello, G. Franzo, F. Priolo et al., *Appl. Phys. Lett.* **81**, 3242 (2002). doi:[10.1063/1.1516235](https://doi.org/10.1063/1.1516235)
7. Y. Kanemitsu, T. Ogawa, K. Shiraishi, K. Takeda, *Phys. Rev. B* **48**, 4883 (1993). doi:[10.1103/PhysRevB.48.4883](https://doi.org/10.1103/PhysRevB.48.4883)
8. K.S. Min, K.V. Shcheglov, C.M. Yang, H.A. Atwater, M.L. Brongersma, A. Polman, *Appl. Phys. Lett.* **69**, 2033 (1996). doi:[10.1063/1.116870](https://doi.org/10.1063/1.116870)

9. J. Linnros, N. Lalic, A. Galeckas, V. Grivickas, *J. Appl. Phys.* **86**, 6128 (1999). doi:[10.1063/1.371663](https://doi.org/10.1063/1.371663)
10. A.G. Nassiopoulou, in *Encyclopedia of Nanoscience and Nanotechnology*, vol. 9, ed. by H.S. Nalwa (American Scientific Publishers, California, 2004), pp. 793–813
11. J. Heitmann, F. Muller, M. Zacharias, U. Gosele, *Adv. Mater.* **17**(7), 795 (2005). doi:[10.1002/adma.200401126](https://doi.org/10.1002/adma.200401126)
12. E. Lioudakis, A.G. Nassiopoulou, A. Othonos, *Appl. Phys. Lett.* **90**, 171103 (2007). doi:[10.1063/1.2728756](https://doi.org/10.1063/1.2728756)
13. A. Othonos, *J. Appl. Phys.* **83**, 1789 (1998). doi:[10.1063/1.367411](https://doi.org/10.1063/1.367411)
14. C.B. Lioutas, N. Vouroutzis, I. Tsiaoussis, N. Frangis, A.G. Nassiopoulou, *Phys. Stat.* **205** (2008)